Aeroacoustics Conferences
26-29 May 2026, Brussels, Belgium
32nd AIAA/CEAS Aeroacoustics Conference (2026)
10.2514/6.2026-3384

Guided jet waves generated by acoustic sources located inside or outside of jets

Christophe Bogey* and Emilian De Staercke†
CNRS, Ecole Centrale de Lyon, INSA Lyon, Universite Claude Bernard Lyon I, Laboratoire de Mécanique des Fluides et d'Acoustique, UMR 5509, 69130 Ecully, France

The generation of guided jet waves (GJW) by acoustic sources located on the axis, at the center of the mixing layer or outside of jets modeled as cylindrical shear layers is investigated using numerical simulations. The shear-layer velocity profile is a hyperbolic-tangent profile with a momentum thickness $\delta_\theta = 0.2r_0$, where r_0 is the jet half-width. Three jet Mach numbers $M = 0.75$, $M = 0.95$ and $M = 1.10$ are considered. The source is axisymmetric and radiates waves at a single frequency, whose propagation is computed by solving the full Euler equations. Axisymmetric GJW entirely or partially confined into the jet, hereafter referred to as duct-like or free-stream GJW, travelling in the upstream or in the downstream directions, can be observed. Their amplitudes upstream and downstream of the source, inside and outside the flow, are quantified. For all Mach numbers, they strongly depend on the Strouhal number, as expected given the GJW dispersion curves, but also on the position of the acoustic source. When the source is located on the jet axis or in the mixing layer, both duct-like and free-stream GJW are generated. The duct-like GJW are, however, less intense for a source in the mixing layer. On the contrary, when the source is outside the jet flow, only free-stream GJW are found. In this case, in addition, no downstream-propagating GJW are obtained for the high subsonic and supersonic Mach numbers.

I. Introduction

The existence of acoustic waves essentially confined in jet flows, called neutral acoustic waves or guided jet waves (GJW) in the literature, has been established in the pioneering work of Tam and Hu [1]. Their properties have been described using linear stability analyses, based on a vortex-sheet model [1, 2] or finite mixing-layer models [3–5], which provided their relation dispersions in the wavenumber-frequency space as well as their eigenfunction profiles in the radial direction. Thus, the GJW have be classified into modes depending on their radial and azimuthal structures. They have also been sorted in different categories depending on the sign of their group velocity and on their magnitude in the shear layer and outside the flow. In brief, they can travel in the upstream or in the downstream directions and they can be entirely or partially contained in the jet. They are then referred to as duct-like GJW in the first case and as free-stream GJW in the second.

As the presence and the specific nature of the GJW have been increasingly recognized in the aeroacoustics community, they were shown to play a crucial role in closing the feedback loops of most resonance phenomena in jet flows [3, 6]. This is particularly true for jets impinging on a flat plate [7–9], for jets interacting with an edge [10] or adjacent to a plate [11], and for screeching shock-containing jets [12, 13]. For free, subsonic and supersonic non-screeching jets, the GJW were also found to be responsible for the generation of tonal-like acoustic peaks near the nozzle exit [14–16], and in the far field in the upstream direction [15, 17, 18]. These peaks were attributed to resonance between upstream- and downstream-propagating GJW [2, 19]. For free jets with laminar nozzle-exit conditions, the GJW were finally reported to excite the shear-layer instability waves near the nozzle [20], thus driving the laminar-turbulence transition.

In spite of the recent advances in the field, important features of the GJW remain little understood. This is the case for the amplitudes of the GJW, given that linear stability analyses usually provide no information on the GJW amplitudes other than their normalized eigenfunction profiles. The mechanisms of generation of the GJW are also unclear, although this is a key point in the occurrence of feedback loops involving upstream-propagating GJW. These GJW are most likely to be fed by the waves emitted by the downstream sources existing in jets, which can be of different kinds and can be located at different positions within the flow [21]. For instance, for all jets, acoustic waves can be

*CNRS Research Scientist, christophe.bogey@ec-lyon.fr, AIAA Associate Fellow.
†PhD Student, emilian.de-staercke@ec-lyon.fr.

produced by the pairings of shear-layer vortices and the merging of the mixing layers at the end of the potential core. For shock-containing jets, waves can result from the interactions between the shear-layer instability waves/coherent structures and the shock cells in the potential core, most probably occurring at the shock tips [22], and from the shock leakage through the mixing-layer regions of low vorticity [23]. For jets impinging on a plate, waves can arise from the impact of turbulent structures on the plate and from shock-turbulence interactions in the wall jets developing over the plate. Finally, for jets adjacent to a plate, upstream-propagating waves can be due to a phenomenon of sound diffraction at the plate trailing edge.

On the basis of the above, numerical simulations are performed in the present study to investigate the generation of GJW from acoustic waves emitted inside or outside jets. In this work, the GJW are considered as the result of a problem of acoustic propagation in presence of a sheared flow. This was previously the case in the theoretical analyses of the scattering of acoustic waves through vortex sheets by Martini et al. [24] and Nogueira et al. [25], in the simulations of the propagation of pressure fluctuations in a jet flow by Bogey and Gojon [7] and Bogey [26]. In recent simulations [27, 28], a monopolar source was also introduced on the axis of jets to generate GJW. Duct-like and free-stream GJW, propagating upstream or downstream, were obtained. For high-subsonic and supersonic Mach numbers, their amplitudes outside the flow were found to peak at the frequencies of the GJW with zero group velocity (ZGV), in accordance with the footprints left by the GJW in the sound spectra near the nozzle of jets.

In the present work, the propagation of the waves radiated by a single-frequency monopolar acoustic source is computed by solving the full Euler equations for three jet Mach numbers, namely two subsonic ones and a supersonic one, and for a wide range of source Strouhal numbers, to deal with GJW of different kinds, belonging to the first two radial GJW modes. The jets are cylindrical shear layers, which are very thick to prevent the development of strong Kelvin-Helmholtz instability waves. The source radiates acoustic waves of low amplitude to avoid non-linear propagation effects. It is placed on the jet axis [27, 28], but also at the center of the jet mixing layer or outside the jet flow. The objective is then to determine, in each of the three cases, which GJW are generated and to describe their properties, namely their amplitude, direction of propagation and free-stream or duct-like nature. In particular, the contributions of the duct-like and free-stream GJW will distinguished using a filtering in the frequency-wavenumber space along the GJW dispersion curves obtained using linear stability analysis.

The paper is organized as follows. In section II, the jet flow conditions and the properties of the acoustic source placed in the flow are defined. The numerical methods and parameters are also documented. In section III, the results obtained for the three Mach numbers are presented. Finally, concluding remarks are given in section IV.

II. Parameters

A. Jet flow

In this study, isothermal round free jets at Mach numbers $M = u_j/c_a = 0.75$, 0.95 and 1.10, where u_j and c_a are the jet velocity and the speed of sound in the ambient medium, are considered. They consist of cylindrical shear layers, surrounded by a medium at rest at temperature $T_a = 293$ K and pressure $p_a = 10^5$ Pa. Following Michalke [29], the radial profile of the axial velocity u_z is defined by the hyperbolic-tangent profile

$$u_z(r) = \frac{u_j}{2}\left\{1 + \tanh\left[\frac{r_0}{4\delta_\theta}\left(\frac{r_0}{r} - \frac{r}{r_0}\right)\right]\right\}$$

where r_0 and δ_θ are the jet half-width and the shear-layer momentum thickness. The jet radial and azimuthal velocities are equal to zero, the jet pressure is equal to p_a and temperature is determined by a Crocco-Busemann relation. The momentum thickness is set to $\delta_\theta = 0.20 r_0$, yielding the velocity profile represented in figure 1(a). This value was chosen to avoid the development of strong Kelvin-Helmholtz (KH) instability waves in the jet flows. Indeed, such waves might pollute the pressure fields and, even worse, lead to shear-layer vortices whose pairings could generate spurious acoustic waves.

The KH instability amplification rates $-\Im(k_z)r_0$ obtained for the azimuthal mode $n_\theta = 0$ for the present shear-layer profile using linear stability analysis for $M = 0.75$, 0.95 and 1.10 are shown in figure 1(b) as a function of the Strouhal number $\mathrm{St}_D = fD/u_j$, where k_z is the axial wavenumber, f is the frequency and $D = 2r_0$. Above $\mathrm{St}_D = 0.47$ for $M = 0.75$, $\mathrm{St}_D = 0.43$ for $M = 0.95$ and $\mathrm{St}_D = 0.38$ for $M = 1.10$, the amplification rates are negative, indicating that no KH instability waves are expected to grow. Below these Strouhal numbers, the amplification rates are weak. For instance, they are approximately ten times smaller than those predicted for $\delta_\theta = 0.05 r_0$, as illustrated in the figure.

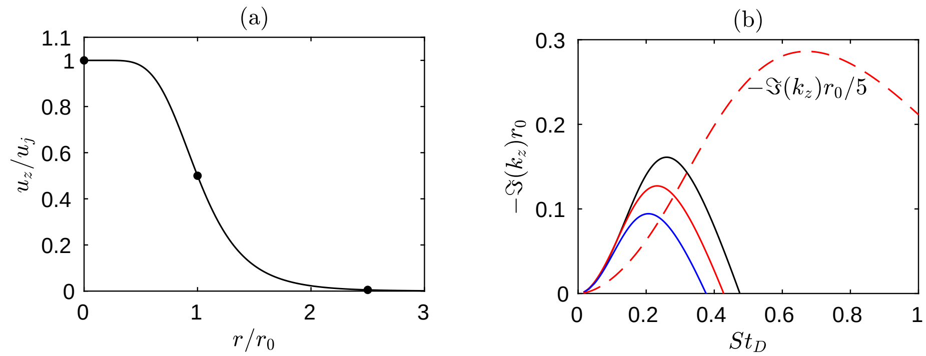

Fig. 1 Representation of (a) the profile of axial velocity u_z/u_j and the three source positions considered and (b) the KH instability growth rates $-\Im(k_z)r_0$ obtained for $n_\theta = 0$ using linear stability analysis for ——— $M = 0.75$, ——— $M = 0.95$ and ——— $M = 1.10$ as a function of St$_D$; – – – $-\Im(k_z)r_0/5$ for $M = 0.95$ and $\delta_\theta = 0.05r_0$.

In that case, therefore, it is most likely that KH instability waves develop, but so slowly that their amplitudes remain small.

The GJW dispersion curves obtained for the azimuthal mode $n_\theta = 0$ for the shear-layer profile using linear stability analysis for $M = 0.75$, 0.95 and 1.10 are represented in figures 2(a-c) in the $k_z - St_D$ space. Due to the thick jet shear layer [3–5], they differ significantly from the dispersion curves predicted using a vortex-sheet model, plotted for comparison. Despite this, as expected [1, 2], the GJW all have negative group velocities $v_g = d\omega/dk_z$ for $M = 0.75$ but can have negative or positive group velocities for $M = 0.95$ and 1.10. Therefore, they can propagate only upstream in the first case, but upstream or downstream in the second. Specific points are marked on the dispersion curves: the limit points L on the sonic line, the inflection points I at Strouhal numbers $St_D^{I,n_r=1} = 0.7314$ and $St_D^{I,n_r=2} = 1.8335$ for $M = 0.75$, and the stationary points, referred to as S_{min} and S_{max} when they correspond to a local minimum or maximum, $St_D^{Smin,n_r=1} = 0.3493$, $St_D^{Smax,n_r=1} = 0.4041$, $St_D^{Smin,n_r=2} = 0.9037$ and $St_D^{Smax,n_r=2} = 0.9716$ for $M = 0.95$ and $St_D^{Smax,n_r=1} = 0.3051$ and $St_D^{Smax,n_r=2} = 0.7154$ for $M = 1.10$, where n_r is the radial mode number. The inflection and stationary points are of particular importance because the GJW have a minimum group velocity at points I and have a zero group velocity at S_{min} and S_{max}, which should give them a high amplitude [27, 28]. These points also enable us to differentiate between the various types of GJW on the dispersion curves. Considering the GJW eigenfunctions obtained using a vortex-sheet model [1, 15] and the comparison with the dispersion curves of acoustic waves in a duct [2], the GJW can be considered to be upstream-propagating free-stream GJW to the right of the points I for $M = 0.75$ and S_{max} for $M = 0.95$ and 1.10, upstream-propagating duct-like GJW to the left of I for $M = 0.75$ and S_{min} for $M = 0.95$. On the basis of the GJW eigenfunctions, the distinctions proposed above between free-stream and duct-like upstream-propagating GJW are well justified for $M = 0.95$, but more arbitrary for $M = 0.75$. Finally, the GJW are downstream-propagating GJW between S_{min} and S_{max} for $M = 0.95$ and to the left of S_{max} for $M = 1.10$. The amplitudes of these waves outside the jet are weak but non negligible near S_{max} but strongly decrease with increasing distance from this point.

B. Acoustic source

To generate sound waves, a single-frequency acoustic source is introduced in the simulations. The source is axisymmetric and is located at the axial position $z = 0$, at three radial positions: at $r = 0$ on the jet axis, at $r = r_0$ at the center of the jet shear layer where $u_z = 0.5u_j$, or at $r = 2.5r_0$ outside the jet flow where $u_z = 0.005u_j$, as illustrated on the velocity profile of figure 1(a). The computations with the source on the jet axis were performed in a previous study [27].

In a (z, r) section, the acoustic source is Gaussian and has a half-width equal to $3\Delta z(z = 0) = 3\Delta r(r = 0) = 0.06r_0$, where Δz and Δr are the grid spacings in the axial and radial directions, which is smaller than the largest acoustic wavelength encountered in this study. The source has a very low amplitude in order to avoid non-linear effects during wave propagation. It radiates at a Strouhal number varying between $St_D = 0.10$ and 2 for $M = 0.75$, $St_D = 0.10$ and 1.2 for $M = 0.95$, and $St_D = 0.05$ and 0.80 for $M = 1.10$. This allows us to deal with GJW belonging to the first two radial axisymmetric GJW modes for the three Mach numbers considered according to the dispersion curves in

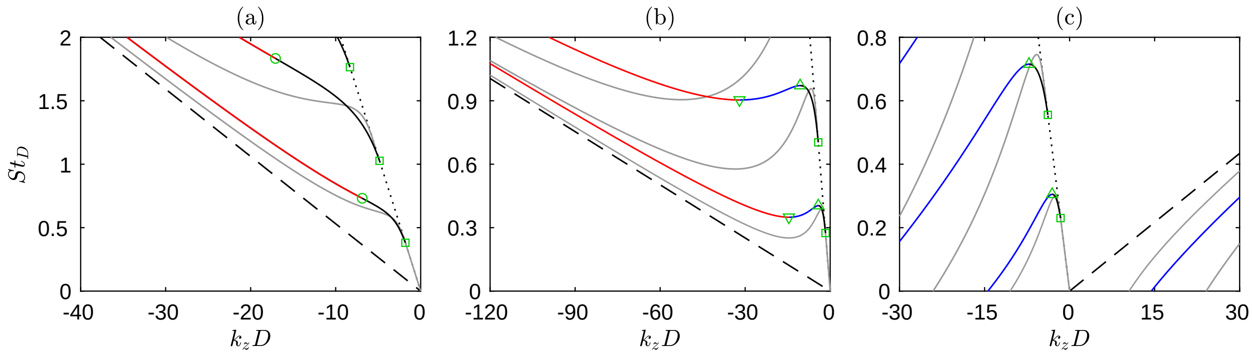

Fig. 2 Dispersion curves obtained for $n_\theta = 0$ using linear stability analysis for (a) $M = 0.75$, (b) $M = 0.95$ and (c) $M = 1.10$: upstream-propagating —— free-stream and —— duct-like GJW, —— downstream-propagating GJW, points □ L, ∘ I, △ S_{max} and ▽ S_{min}; —— dispersion curves for a vortex sheet; − − − $k_z = \omega/(u_j - c_0)$, ····· $k_z = -\omega/c_0$.

figure 2. To accurately describe the variations of the GJW properties, the number of source Strouhal numbers n_{source} is significant, and is equal to 192 for $M = 0.75$, 271 for $M = 0.95$ and 187 for $M = 1.10$. In the last two cases, the source frequencies are specially clustered around the Strouhal numbers of the stationary points S_{min} and S_{max} of the GJW dispersion curves, around which tonal-like peak components appear.

C. Numerical methods

The computations are carried out by solving the full Euler equations in cylindrical coordinates (r, θ, z) using the same numerical framework based on explicit high-order schemes as in previous simulations of spatially-developing [15, 20] and temporally-developing [30, 31] round jets. The axis singularity is taken into account by the method of Mohseni and Colonius [32]. Fourth-order eleven-point centered finite differences are used for spatial discretization, and a second-order six-stage Runge-Kutta algorithm is implemented for time integration [33]. A twelfth-order centered filter is applied explicitly to the flow variables every time step to remove grid-to-grid oscillations. Non-centered finite differences and filters are used at the grid lateral boundaries [34], where the radiation conditions of Tam and Dong [35] are applied. Periodic conditions are implemented at the inflow and outflow boundaries. Near these boundaries, sponge zones based on grid stretching and Laplacian filtering are built to move the periodic conditions very far from the region where wave propagation will be investigated.

D. Numerical parameters

The grids used in the simulations are symmetrical relative to the source position $z = 0$. Excluding the 260-point inflow and outflow sponge zones, they extend axially between $z = -30r_0$ and $30r_0$ and radially out to $r = 25r_0$. Over $-30r_0 \le z \le 30r_0$, the axial mesh spacing Δz is uniform and equal to $0.02r_0$. In the radial direction, the mesh spacing Δr is also equal to $0.02r_0$ between $r = 0$ and $1.2r_0$ when the source is located at $r = 0$ or at $r = r_0$, and between $r = 0$ and $2.7r_0$ when the source is at $r = 2.5r_0$. It then increases farther from the jet axis, reaching $\Delta r = 0.16r_0$ between $r = 6.5r_0$ and $r = 16r_0$ and $\Delta r = 0.32r_0$ for $r \ge 21.6r_0$. The grid thus contains $N_z = 3,519$ points in the axial direction and $N_r = 235$ or 302 points in the radial direction depending on the source position. Given that the jet flow, the acoustic sources and the sound waves are axisymmetric, only $N_\theta = 2$ points are used in the azimuth.

For a source radiating over $0.38 \le St_D \le 0.4075$ and $0.90 \le St_D \le 0.975$ for $M = 0.95$ and over $0.66 \le St_D \le 0.735$ for $M = 1.10$, upstream- and downstream-propagating GJW can both exist. To avoid spurious reflections in the sponge zones, the simulations are carried out using grids longer in the axial direction, containing more points in the central region where $\Delta z = 0.02r_0$. This region extends between $\pm 70r_0$ for $M = 0.95$ and $\pm 90r_0$ for $M = 1.10$, requiring 4,000 and 6,000 additional points, respectively.

Finally, the simulations are performed with an OpenMP-based in-house solver using a time step $\Delta t = CFL \times \Delta r(r = r_0)/c_a$ with $CFL = 0.7$ for $M = 0.75$, 0.65 for $M = 0.95$ and 0.6 for $M = 1.10$ ensuring numerical stability. Pressure is recorded in the plane $\theta = 0$ at every third point in the axial direction and at every second point in the radial direction at a frequency corresponding to $\mathrm{St}_D = 6.4$, and at $r = 0$ and $r = 2r_0$ at every second point between $z = \pm 30r_0$ at a double frequency. The simulation times are of the order of $300r_0/c_a$. They are long because the GJW, especially near the points S_{min} and S_{max} in the dispersion curves of figures 2(b,c), can propagate at a group velocity much lower than the ambient speed of sound.

III. Results

Results are provided for the three jet Mach numbers to illustrate the various GJW generated by the acoustic sources at the different distances to the jet axis. In the three cases, pressure snapshots are provided for source Strouhal numbers inside or just above or below the allowable frequency ranges of the upstream-propagating free-stream axisymmetric GJW belonging to radial mode $n_r = 2$, in which no KH instability waves can develop, according to the curves in figures 1(b) and 2 obtained using linear stability analysis. Then, the sound pressure levels calculated upstream of the source at $z = -15r_0$ and downstream at $z = 15r_0$, inside the jet at $r = 0$ and outside at $r = 2r_0$, are presented to quantify the amplitudes and determine the free-stream or duct-like natures of the GJW. They are normalized by the sound levels obtained without flow. For $M = 0.95$, the contributions of the free-stream and duct-like GJW upstream of the source will be distinguished using a filtering in the frequency-wavenumber space along selected segments of the GJW dispersion curves.

A. Mach number of 0.75

The pressure snapshots obtained for nine source Strouhal numbers St_D between 0.98 and 1.86 for $M = 0.75$ are provided in figure 3 for the source at $r = 0$, in figure 4 for the source at $r = r_0$ and in figure 5 for the source at $r = 2.5r_0$. The levels are normalized by the r.m.s. values of pressure fluctuations obtained without flow at $r = 0$ and $z = 15r_0$. They are represented using logarithmic scales ranging over 4, 3 and 2 orders of magnitude, respectively. For comparison with the source frequencies, it is noted that the Strouhal numbers of the limit and inflection points in the dispersion curve of the axisymmetric GJW of radial mode $n_r = 2$ are equal to $St_D^{L,n_r=2} = 1.0267$ and $St_D^{I,n_r=2} = 1.8335$ for the present Mach number in figure 2(a).

GJW are observed upstream of the source in all cases, but downstream in none, in agreement with the dispersion curves in figure 2(a). The properties of the upstream-propagating GJW, however, strongly depend on the source position.

For the source on the jet axis, in figure 3, strong GJW are found for all Strouhal numbers. Their radial structures vary with the frequency, as was reported previously [27]. For $St_D = 0.98 < St_D^{L,n_r=2}$, in figure 3(a), the GJW are duct-like GJW belonging to mode $n_r = 1$. As the frequency increases, GJW with a node in their radial profiles extending farther than $r = r_0$ appear. They are free-stream GJW of mode $n_r = 2$. Finally, for $St_D = 1.86 > St_D^{I,n_r=2}$, in figure 3(i), the GJW are duct-like GJW of mode $n_r = 2$. Therefore, placing the source on the jet axis allows the generation of all GJW, regardless of their free-stream or duct-like nature.

For the source located at $r = 2.5r_0$, in figure 5, the results differ significantly. In this case, the amplitudes of the GJW are much lower. All the GJW also seem to have a radial support extending beyond $r = r_0$ and no GJW fully contained in the jet flow can be seen. This is particularly true for the two Strouhal numbers $St_D = 0.98$ and 1.86 for which only free-stream GJW of modes $n_r = 2$ and 3 are visible in figures 5(a) and 5(i), but for which strong duct-like GJW of modes $n_r = 1$ and 2 are found in figures 3(a) and 3(i) for the on-axis source. This suggests that an acoustic source outside the jet flow can only generate free-stream GJW.

Finally, for the source located at $r = r_0$ at the center of the jet shear layer, the pressure fields in figure 13 exhibit GJW with amplitudes in between those obtained for the sources inside and outside the flow. As in figure 3, GJW entirely contained within the jet flow can be observed. In particular, duct-like GJW of modes $n_r = 1$ and 2 appear in figures 4(a) and 4(i), resembling those in figures 3(a) and 3(i) for the on-axis source. In the other figures, when the source Strouhal number lies within the frequency range of the free-stream GJW of mode $n_r = 2$, the contributions of duct-like GJW of mode $n_r = 1$ to the pressure fields are weak, as in figure 4(c), or may even be hard to detect, as in figures 4(e-h), whereas such GJW are clearly superimposed on free-stream GJW of mode $n_r = 2$ in figures 3(e-h), the two kinds of GJW having different wavelengths. Thus, an acoustic source in the jet mixing layer can lead to the formation both duct-like and free-stream GJW, but it may result in weaker or fewer duct-like GJW than a source inside the jet.

To quantify the intensities of the GJW, the sound pressure levels obtained at $z = -15r_0$ at $r = 0$ and $r = 2r_0$ are shown. They are subtracted from the baseline levels calculated without flow at $z = -15r_0$ at $r = 0$. They are represented as a function of the Strouhal number in figure 6(a) for the source at $r = 0$, in figure 6(b) for the source at $r = r_0$ and in figure 6(c) for the source at $r = 2.5r_0$. The frequencies of the inflexion points in the GJW dispersion curves, where the GJW have a minimum zero group, are indicated.

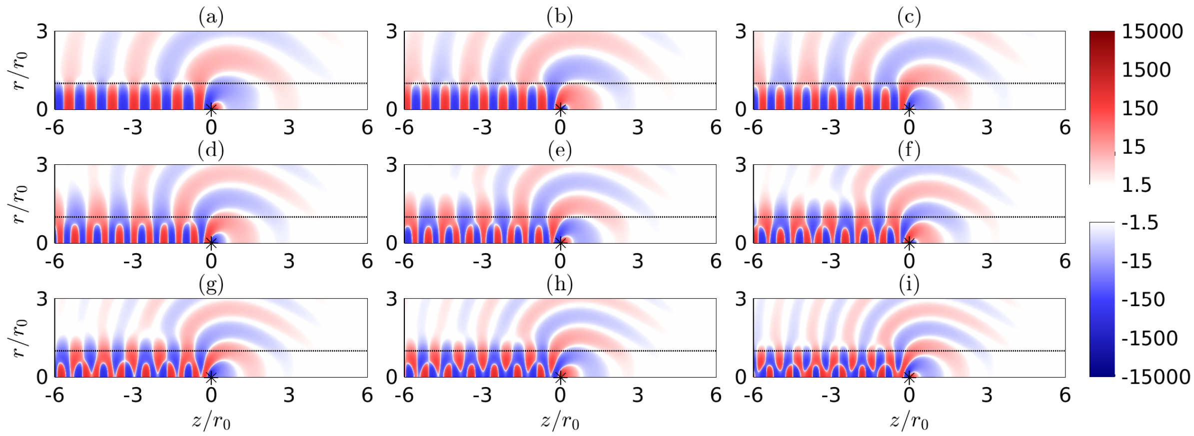

Fig. 3 **Pressure fluctuations obtained for $M = 0.75$ using a source $*$ at $z = 0$ and $r = 0$ for Strouhal numbers (a) 0.98, (b) 1.14, (c) 1.22, (d) 1.30, (e) 1.38, (f) 1.46, (g) 1.54, (h) 1.70 and (i) 1.86; ····· $r = r_0$. The levels are normalized by the r.m.s. values of pressure fluctuations obtained without flow at $15r_0$ from the source.**

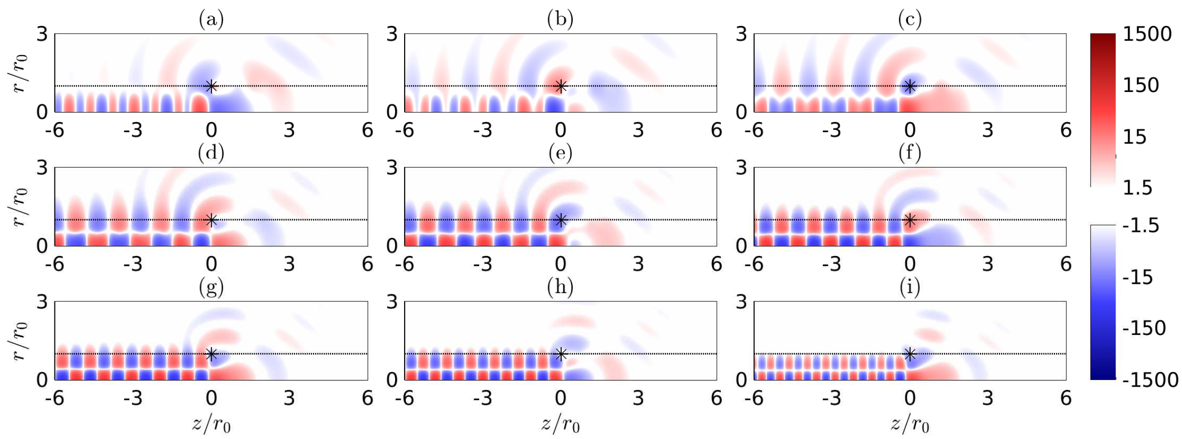

Fig. 4 **Pressure fluctuations obtained for $M = 0.75$ using a source $*$ at $z = 0$ and $r = r_0$ for the same Strouhal numbers as in figure 3; ····· $r = r_0$. The levels are normalized by the r.m.s. values of pressure fluctuations obtained without flow at $r = 0$ and $z = 15r_0$.**

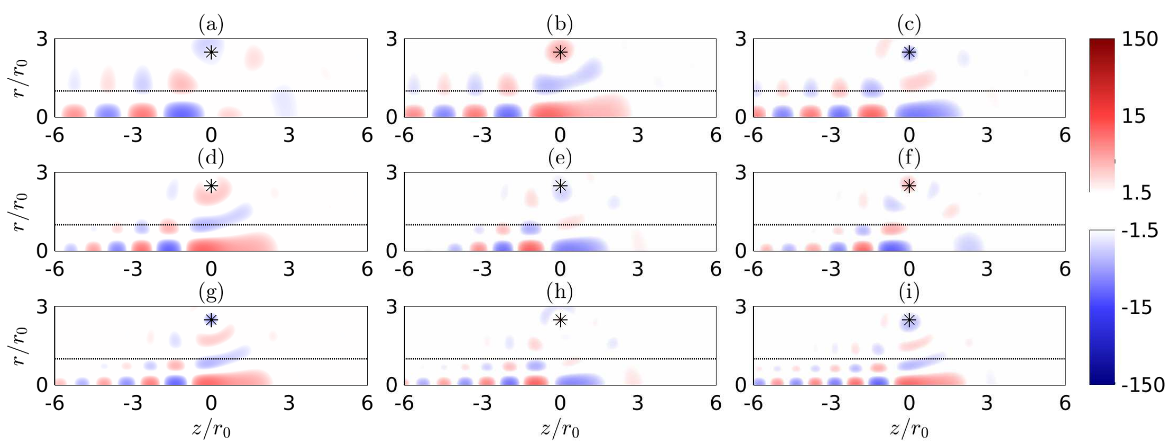

Fig. 5 **Pressure fluctuations obtained for $M = 0.75$ using a source $*$ at $z = 0$ and $r = 2.5r_0$ for the same Strouhal numbers as in figure 3; ····· $r = r_0$. The levels are normalized by the r.m.s. values of pressure fluctuations obtained without flow at $r = 0$ and $z = 15r_0$.**

Outside the flow, the levels (in red) are low and show three bumps which are similar in the three cases. The bumps are respectively due to the contributions of free-stream GJW of radial modes $n_r = 1$, 2 and 3 to the jet near field. Inside the flow, the levels (in black) depend on the source position. When the source is on the jet axis, the levels remain high and greater than 30 dB for $St_D \geq 0.5$ in figure 6(a), whereas for the source outside the jet flow they do not exceed 15 dB and oscillate in the same way as the levels at $r = 2r_0$ in figure 6(c). This confirms the presence of strong duct-like GJW for all St_D above 0.5 in the first case, and the absence of such waves in the second. When the source is in the jet mixing layer, the levels on the jet axis in figure 6(b) fluctuate but are much higher than those at $r = 2r_0$. Therefore, duct-like GJW exist but their intensity varies with the frequency.

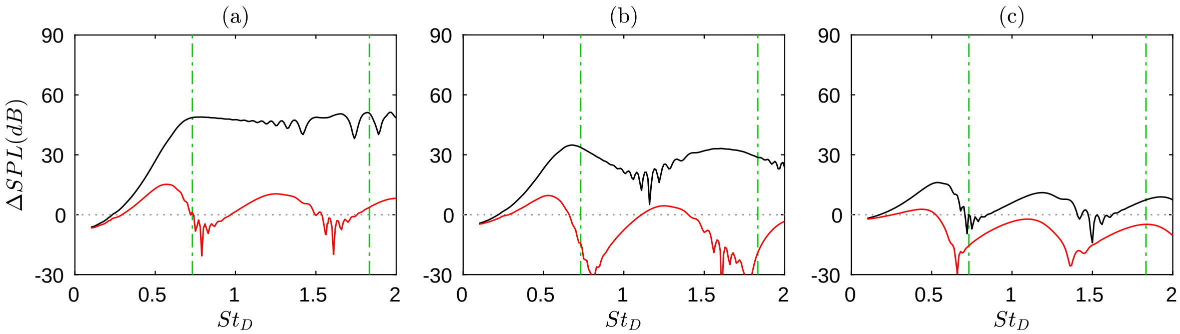

Fig. 6 Strouhal number variations of the sound pressure levels obtained for the jet at $M = 0.75$ at $z = -15r_0$ and ——— $r = 0$ and ——— $r = 2r_0$, subtracted from the no-flow reference levels at $z = -15r_0$ and $r = 0$, using a source at (a) $r = 0$, (b) $r = r_0$ and (c) $r = 2.5r_0$; - · - · $St_D^{I,n_r=1}$ and $St_D^{I,n_r=2}$, from left to right.

B. Mach number of 0.95

The pressure snapshots obtained for nine Strouhal numbers St_D between 0.65 and 1.03 for $M = 0.95$ are given in figure 7 for the source at $r = 0$, in figure 8 for the source at $r = r_0$ and in figure 9 for the source at $r = 2.5r_0$. As previously, the levels are normalized by the no-flow r.m.s. pressure values at $r = 0$ and $z = 15r_0$, and are represented over 4, 3 and 2 orders of magnitude. For the discussion below, it is worth noting that the Strouhal numbers of the limit and the stationary points in the dispersion curve of the axisymmetric GJW of mode $n_r = 2$ for $M = 0.95$ are equal to $St_D^{L,n_r=2} = 0.7033$, $St_D^{Smin,n_r=2} = 0.9037$ and $St_D^{Smax,n_r=2} = 0.9716$ in figure 2(b).

GJW are observed upstream of the source in all cases, with amplitudes and nature strongly depending on the frequency and the source position. Downstream, they appear only for the source at $r = 0$ or at $r = r_0$, between $St_D = 0.905$ and $St_D = 0.97$, that is within the frequency range $St_D^{Smin,n_r=2} \leq St_D \leq St_D^{Smax,n_r=2}$ of the downstream-propagating GJW of mode $n_r = 2$, as expected.

The variations of the GJW properties with the frequency for the source on the jet axis in figure 7 are discussed in a recent paper [28]. In brief, upstream, only duct-like GJW are found in figure 7(a) for $St_D < St_D^{L,n_r=2}$ and in figure 7(i) for $St_D > St_D^{Smax,n_r=2}$, and both duct-like and free-stream GJW exist in figures 7(b-h) for $St_D^{L,n_r=2} < St_D < St_D^{Smax,n_r=2}$. Downstream, GJW are visible in figures 7(e-h) for $St_D^{Smin,n_r=2} \leq St_D \leq St_D^{Smax,n_r=2}$. The amplitudes of the GJW are strongest near the frequencies of the stationary points.

For the source at $r = 2.5r_0$, in figure 9, as was reported previously for $M = 0.75$, the amplitudes of the GJW are much lower and only free-stream GJW can be seen upstream of the source, their free-stream nature being revealed by their long wavelengths compared with those of the duct-like GJW. There are apparently no GJW downstream. Therefore, the downstream-propagating GJW located between the stationary points S_{min} and S_{max} in the GJW dispersion curves do not seem to be generated for a source located outside the jet. This can be explained by the fact that, although these waves are not entirely confined within the jet, they cannot be considered fully as free-stream GJW given that their amplitudes are very low beyond $r = r_0$ according to the GJW eigenfunctions [20].

Finally, for the source at $r = r_0$, in figure 8, downstream-propagating GJW appear as in figure 7 for the on-axis source. Upstream of the source, with one exception, the pressure fields exhibit free-stream GJW but no duct-like GJW, the exception being in figure 8(e) for $St_D = 0.905 \simeq St_D^{Smin,n_r=2}$. This suggests that a source in the mixing layer cannot generate duct-like GJW to the left of the points S_{min} in the dispersion curves, except for the less confined ones [20] which are very close to S_{min}.

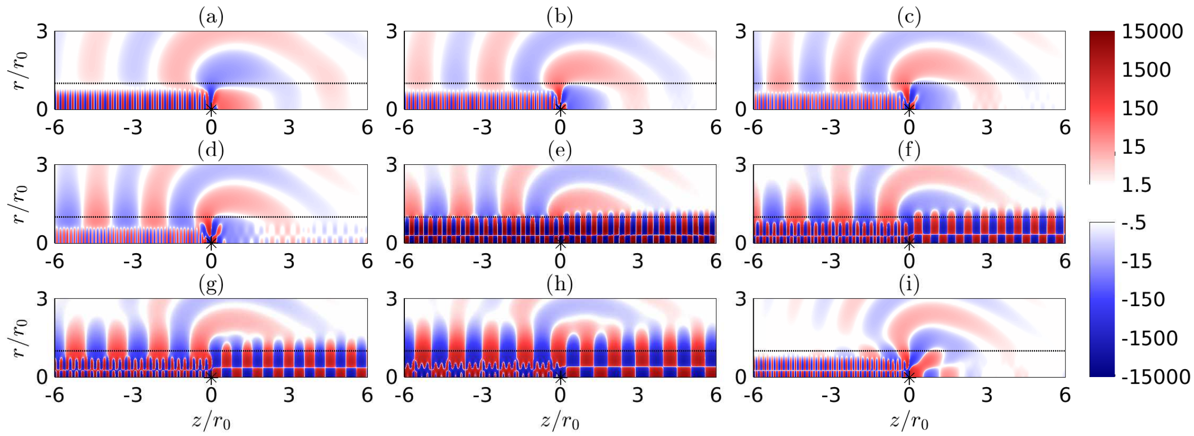

Fig. 7 Pressure fluctuations obtained for $M = 0.95$ using a source $*$ at $z = 0$ and $r = 0$ for Strouhal numbers (a) 0.65, (b) 0.74, (c) 0.805, (d) 0.855, (e) 0.905, (f) 0.93, (g) 0.95, (h) 0.97 and (i) 1.03; ····· $r = r_0$. The levels are normalized by the r.m.s. values of pressure fluctuations obtained without flow at $15r_0$ from the source.

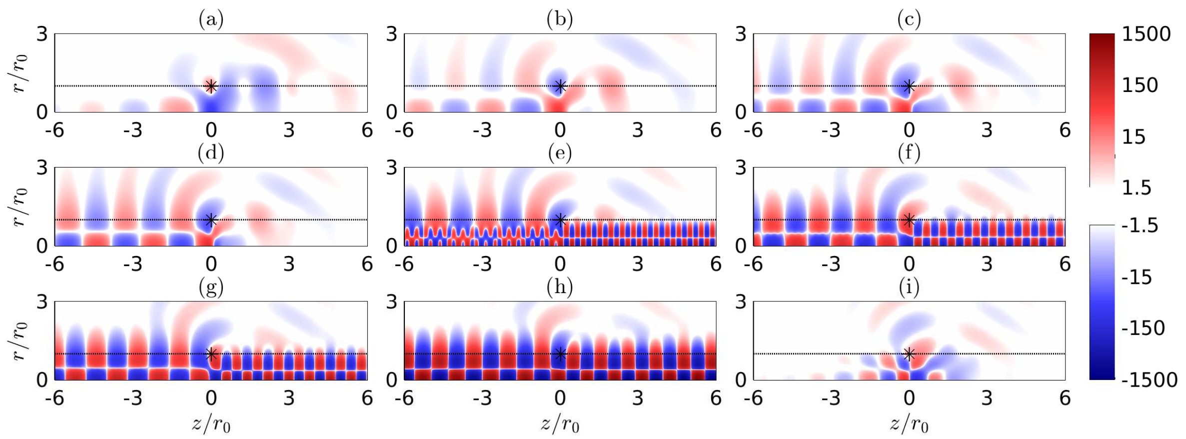

Fig. 8 Pressure fluctuations obtained for $M = 0.95$ using a source $*$ at $z = 0$ and $r = r_0$ for the same Strouhal numbers as in figure 7; ····· $r = r_0$. The levels are normalized by the r.m.s. values of pressure fluctuations obtained without flow at $r = 0$ and $z = 15r_0$.

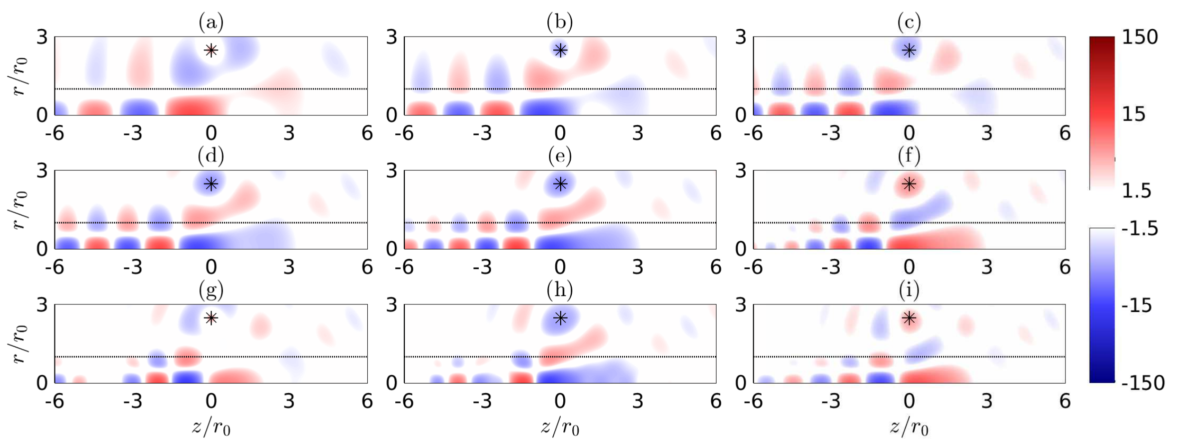

Fig. 9 Pressure fluctuations obtained for $M = 0.95$ using a source $*$ at $z = 0$ and $r = 2.5r_0$ for the same Strouhal numbers as in figure 7; ····· $r = r_0$. The levels are normalized by the r.m.s. values of pressure fluctuations obtained without flow at $r = 0$ and $z = 15r_0$.

The sound pressure levels obtained at $z = \pm 15r_0$ at $r = 0$ and $r = 2r_0$ are represented as a function of the Strouhal number in figures 10(a,d) for the source at $r = 0$, in figures 10(b,e) for the source at $r = r_0$ and in figures 10(c,f) for the source at $r = 2.5r_0$. They are subtracted from the baseline levels calculated without flow at $z = \pm 15r_0$ at $r = 0$. The results at $z = -15r_0$ are shown in the top figures, those at $z = 15r_0$ in the bottom figures. The frequencies of the stationary points in the GJW dispersion curves, where the GJW have a zero group velocity, are displayed. Tonal-like peaks emerge near these frequencies, as discussed recently [28].

Downstream of the source, in figures 10(d-f), a large bump associated with the KH instability waves developing in the jet mixing layer emerge at low frequencies. Apart from the bump, the results are similar for the sources located at $r = 0$ and $r = r_0$, but differ in the third case. In the first two cases, in figures 10(d,e), the levels on the jet axis are strong and greater than 40 dB between $St_D^{Smin,n_r=1}$ and $St_D^{Smax,n_r=1}$ and $St_D^{Smin,n_r=2}$ and $St_D^{Smax,n_r=2}$, whereas those at $r = 2r_0$ are only significant near $St_D^{Smax,n_r=1}$ and $St_D^{Smax,n_r=2}$. Therefore, they are due to GJW which are not fully confined (near $St_D^{Smax,n_r=1,2}$) or fully confined (otherwise) within the jet. For the source outside the flow, in figure 10(f), no GJW contributions emerge except near $St_D^{Smax,n_r=1}$ and $St_D^{Smax,n_r=2}$, both at $r = 0$ and $r = 2r_0$. This confirms the free-stream nature of the downstream-propagating GJW near the points S_{max} in the dispersion curves.

Upstream of the source, in figures 10(a-c), the levels outside the jet vary with the frequency in a reverse saw-tooth manner with gradual increases followed by sharp decreases at $St_D^{Smax,n_r=1,2}$. They result from the upstream-propagating free-stream GJW near the sonic line $k_z = -\omega/c_0$, which are cut off at the above Strouhal numbers. The teeth are, however, rounded in figure 10(c) for the source outside the jet. This can be explained by the fact that the GJW mentioned above extend less in the radial direction when they are close to the points S_{max} in the dispersion curves. Thus, they cannot be generated efficiently by an external source.

Finally, the levels on the jet axis upstream of the source are different in the three cases. For the on-axis source, in figure 10(a), the levels vary in a saw-tooth manner with sudden rises at $St_D^{Smin,n_r=1,2}$ followed by gradual decreases. For the in-mixing-layer source, in figure 10(b), they are especially strong between $St_D^{Smin,n_r=1}$ and $St_D^{Smax,n_r=1}$, two Strouhal numbers at which tonal-like peaks are reached, and then fluctuate in a reverse saw-tooth manner with a fall at $St_D^{Smax,n_r=2}$. For the external source, in figure 10(c), they exhibit two reverse saw-tooth patterns peaking at $St_D^{Smax,n_r=1}$ and $St_D^{Smax,n_r=2}$.

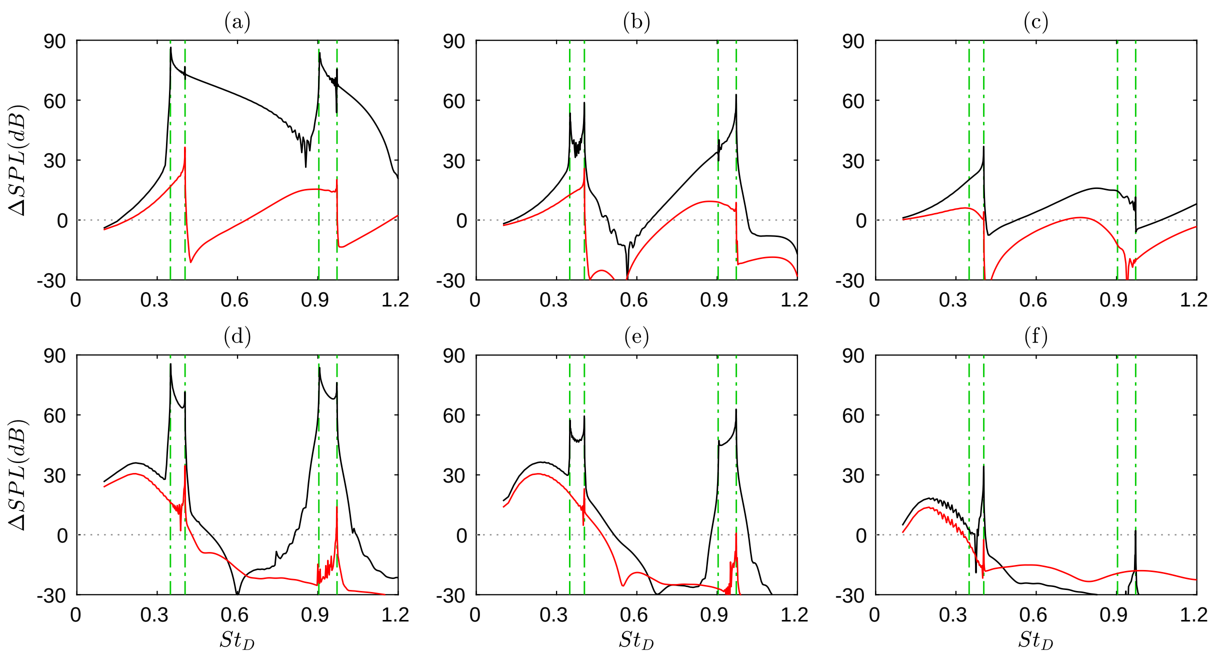

Fig. 10 Strouhal number variations of the sound pressure levels obtained for the jet at $M = 0.95$ (a-c) at $z = -15r_0$ and (d-f) at $z = 15r_0$ at —— $r = 0$ and —— $r = 2r_0$, subtracted from the no-flow reference levels at $z = \pm 15r_0$ and $r = 0$, using a source at (a,d) $r = 0$, (b,e) $r = r_0$ and (c,f) $r = 2.5r_0$; - · - $St_D^{Smin,n_r=1}$, $St_D^{Smax,n_r=1}$, $St_D^{Smin,n_r=2}$ and $St_D^{Smax,n_r=2}$, from left to right.

To explain the trends described above, the contributions from the free-stream and duct-like GJW upstream of the source are separated and and examined individually. This is done by applying a frequency-wavenumber filtering to the pressure signals along selected segments of the dispersion curves of figure 2(b), namely the segments between the limit points L and the stationary points S_{max} for the free-stream GJW and the segments extending to the left of the stationary points S_{min} for the duct-like GJW.

The sound pressure levels thus obtained at $z = -15r_0$ at $r = 0$ for the free-stream GJW belonging to the radial modes $n_r = 1$, 2 and 3 and for the duct-like GJW of modes $n_r = 1$ and 2 are represented as a function of the Strouhal number in figure 11 for the three source positions. For clarity, the curves are offset by -15 dB relative to the total sound pressure levels. For the source at $r = 2.5r_0$, in figure 11(c), the contributions of the duct-like GJW are negligible, providing further evidence that an acoustic source outside the flow can only produce free-stream GJW. In the two other cases, in figures 11(a,b), the contributions of the duct-like and free-stream GJW are both significant, varying, respectively, in a reverse saw-tooth manner and in a saw-tooth manner. The contributions of the duct-like GJW are strong and predominant in figure 11(a), but they are much lower and do not exceed those of the free-stream GJW in figure 11(b). This supports the observation made for $M = 0.75$ that a source in the jet shear layer generates weaker duct-like GJW than a source inside the jet potential core.

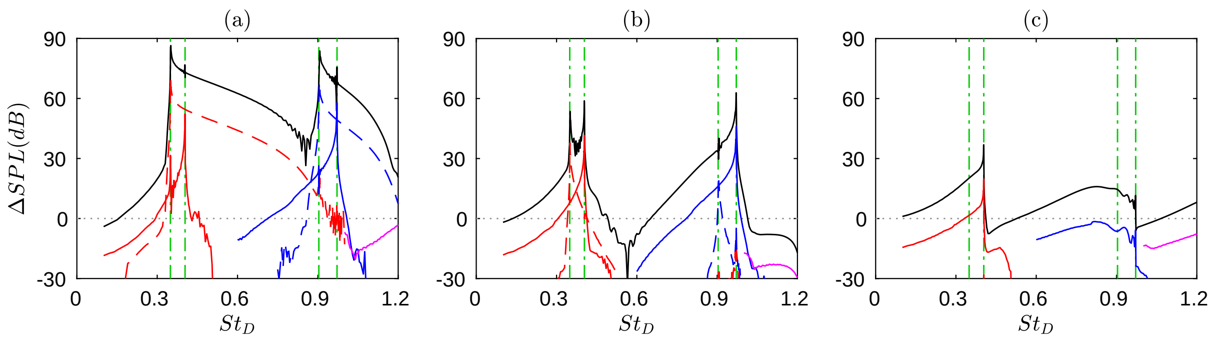

Fig. 11 Strouhal number variations ——— of the sound pressure levels obtained for $M = 0.95$ at $z = -15r_0$ and $r = 0$, subtracted from the no-flow reference levels, using a source at (a) $r = 0$, (b) $r = r_0$ and (c) $r = 2.5r_0$; $\Delta SPL - 15$ dB obtained for the ——— free-stream and – – – duct-like GJW of mode $n_r = 1$, ——— free-stream and – – – duct-like GJW of mode $n_r = 2$, ——— free-stream GJW of mode $n_r = 3$; – · – $St_D^{Smin,n_r=1}$, $St_D^{Smax,n_r=1}$, $St_D^{Smin,n_r=2}$ and $St_D^{Smax,n_r=2}$, from left to right.

C. Mach number of 1.10

The pressure snapshots obtained for nine Strouhal numbers St_D between 0.40 and 0.73 for $M = 1.10$ are given in figure 12 for the source at $r = 0$, in figure 13 for the source at $r = r_0$ and in figure 14 for the source at $r = 2.5r_0$. The levels are normalized and represented in the same way as in figures 3-5 and 7-9. The Strouhal numbers of the limit and stationary points in the dispersion curve of the axisymmetric GJW of mode $n_r = 2$ for $M = 1.10$ are equal to $St_D^{L,n_r=2} = 0.5554$ and $St_D^{Smax,n_r=2} = 0.7154$ in figure 2(c).

Upstream of the source, free-stream GJW with one node in their radial profiles are observed for the three source positions for the seven Strouhal numbers within the frequency range of the upstream-propagating free-stream GJW of mode $n_r = 2$. For $St_D = 0.40$, in figure 12(a), 13(a) and 14(a), acoustic waves appear in the jet flow, but their amplitudes decrease with the distance to the source, as expected given that $St_D < St_D^{L,n_r=2}$. A similar observation is made in figures 12(i), 13(i) and 14(i) for $St_D = 0.73 > St_D^{Smax,n_r=2}$. Therefore, the upstream-propagating GJW lying between the points L and S_{max} in the GJW dispersion curves can be generated regardless of the source position. It is reminded that no duct-like upstream-propagating GJW can exist for a supersonic Mach number.

Downstream, GJW are found for all frequencies for the source at $r = 0$, for the first eight frequencies for the source at $r = r_0$ and never for the source at $r = 2.5r_0$. For the on-axis source, in figure 12, GJW with different radial extents and axial wavelengths seem to be superimposed. The GJW extending farther than $r > r_0$ have large wavelengths, and disappear for $St_D = 0.73 > St_D^{Smax,n_r=2}$ in figures 12(i). This implies that they are the GJW immediately to the left of the point S_{max} on the dispersion curve of the GJW mode $n_r = 2$. The strong duct-like GJW also obtained for all frequencies most likely correspond to the other downstream-propagating GJW possible in the present cases, which are those belonging to the radial modes $n_r > 2$ with $k_z < 0$ and those with $k_z > 0$ in the dispersion curves of figure 2(c).

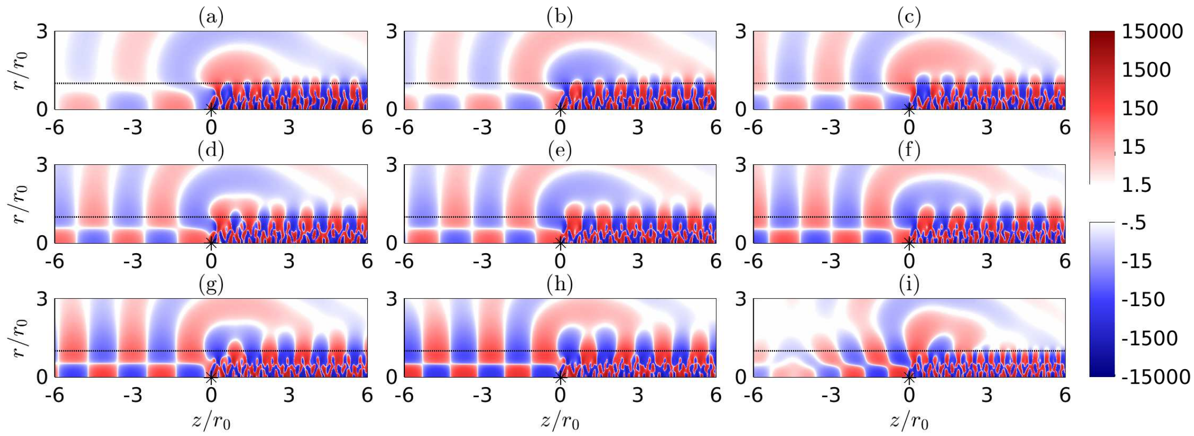

Fig. 12 **Pressure fluctuations obtained for $M = 1.10$ using a source at $z = 0$ and $r = 0$ for Strouhal numbers (a) 0.40, (b) 0.55, (c) 0.625, (d) 0.655, (e) 0.67, (f) 0.685, (g) 0.70, (h) 0.71 and (i) 0.73; ····· $r = r_0$. The levels are normalized by the r.m.s. values of pressure fluctuations obtained without flow at $15r_0$ from the source.**

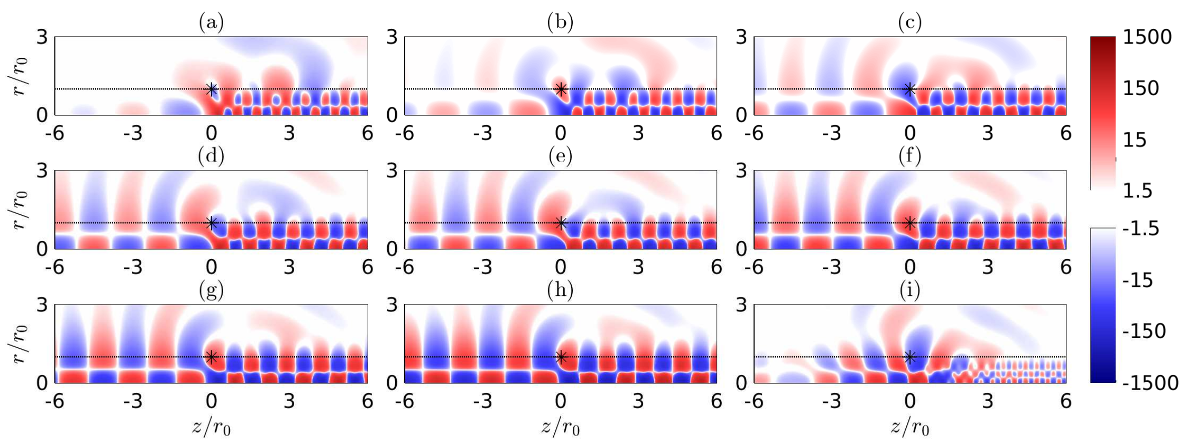

Fig. 13 **Pressure fluctuations obtained for $M = 1.10$ using a source $*$ at $z = 0$ and $r = r_0$ for the same Strouhal numbers as in figure 12; ····· $r = r_0$. The levels are normalized by the r.m.s. values of pressure fluctuations obtained without flow at $r = 0$ and $z = 15r_0$.**

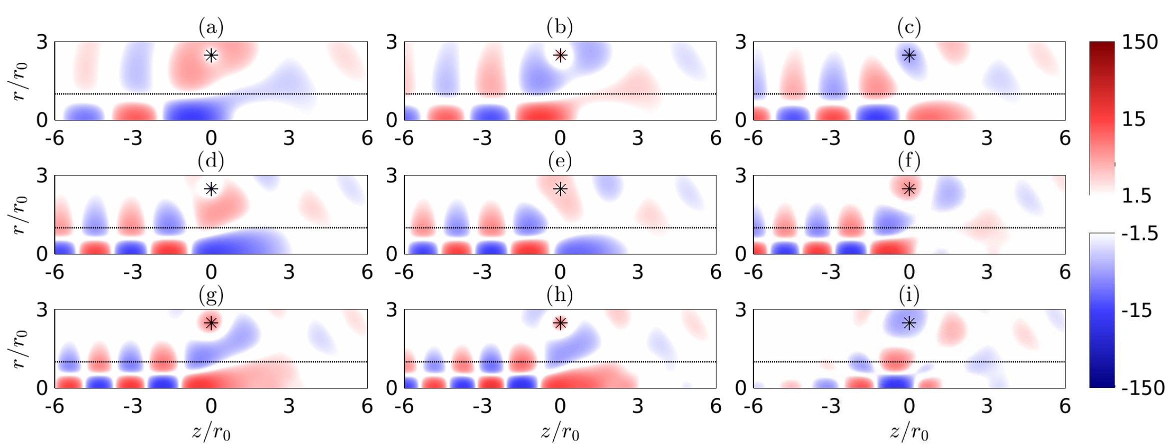

Fig. 14 **Pressure fluctuations obtained for $M = 1.10$ using a source $*$ at $z = 0$ and $r = 2.5r_0$ for the same Strouhal numbers as in figure 12; ····· $r = r_0$. The levels are normalized by the r.m.s. values of pressure fluctuations obtained without flow at $r = 0$ and $z = 15r_0$.**

For the in-mixing layer source, in figure 13, only the free-stream GJW of mode $n_r = 2$, clearly extending beyond $r = r_0$, remain in the pressure fields. Finally, for the external source, in figure 14, no GJW form downstream. These results further confirm that the GJW that can be generated by an acoustic source at a specific distance from the jet axis depend on their radial extent. As this distance increases, the more confined GJW are no longer produced.

The sound pressure levels obtained at $z = \pm 15 r_0$ at $r = 0$ and $r = 2r_0$ are represented as a function of the Strouhal number in figures 15(a,d) for the source at $r = 0$, in figures 15(b,e) for the source at $r = r_0$ and in figures 15(c,f) for the source at $r = 2.5r_0$. They are subtracted from the no-flow baseline levels. In the same way as in figure 10, the results at $z = -15r_0$ are shown in the top figures, those at $z = 15r_0$ in the bottom figures. The frequencies of the waves with zero group velocity in the GJW dispersion curves are depicted.

The levels obtained upstream in figures 15(a-c) show similar variations with the frequency for the two measurement points and for the three source positions. Two reverse saw-tooth patterns peaking at $St_D^{Smax,n_r=1}$ and $St_D^{Smax,n_r=2}$ are observed. They are caused by the presence of only free-stream GJW. The downstream levels attributable to GJW in figures 15(d-f) are weak outside the jet for the three source positions, except near $St_D^{Smax,n_r=1,2}$ for the on-axis and in-mixing-layer sources where the contributions of the downstream-propagating free-stream GJW immediately to left of the points S_{max} in the GJW dispersion curves are non negligible according to their eigenfunctions [20]. The levels obtained on the jet axis in figure 15(f) exhibit very similar features. Those in figures 15(d) and 15(e) are much stronger. They are mainly due, respectively, to the duct-like GJW and to the GJW to left of the points S_{max} mentioned previously.

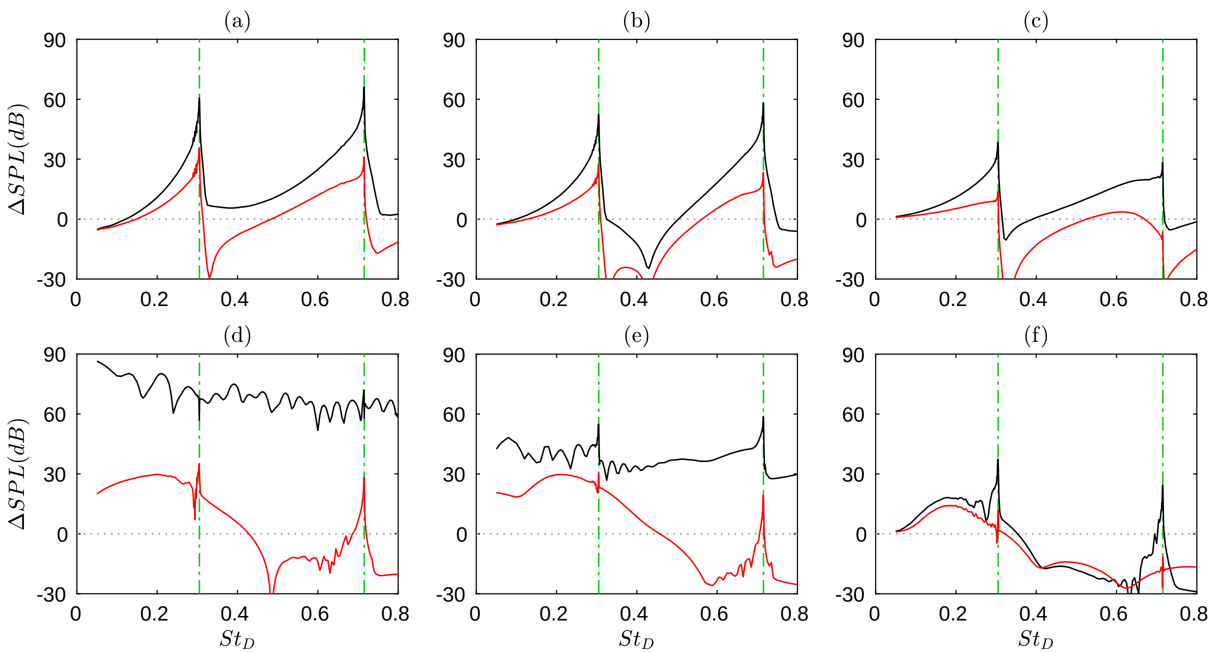

Fig. 15 Strouhal number variations of the sound pressure levels obtained for the jet at $M = 1.10$ (a-c) at $z = -15r_0$ and (d-f) at $z = 15r_0$ at ——— $r = 0$ and ——— $r = 2r_0$, subtracted from the no-flow reference levels at $z = \pm 15r_0$ and $r = 0$, using a source at (a,d) $r = 0$, (b,e) $r = r_0$ and (c,f) $r = 2.5r_0$; – · – $St_D^{Smax,n_r=1}$ and $St_D^{Smax,n_r=2}$, from left to right.

IV. Conclusion

In this paper, the generation of GJW by acoustic sources placed at different distances from the jet axis has been investigated for Mach numbers 0.75, 0.95 and 1.10 by performing numerical simulations of linear sound propagation. It is shown that GJW can be obtained regardless of whether the source is located inside or outside the jet. However, while an on-axis source can generate all possible GJW for a given jet, only a part, namely the less confined ones, can be produced as the source is farther away from the axis. Thus, the GJW that are fully contained inside the jet become weaker and fewer and, for a source outside the jet, only free-stream GJW persist. A notable consequence of this is the absence of upstream-propagating duct-like GJW in all cases, and the absence of downstream-propagating GJW for high subsonic and supersonic Mach numbers when the acoustic source is located outside the jet.

The present results are important given the key role of GJW in the formation of feedback loops in jets. They demonstrate that the nature of the acoustic waves closing the loops depends on the position of the source generating them. Specifically, for a sound source located outside the flow, feedback loops cannot involve duct-like GJW or downstream-propagating GJW. Instead, they could rely on free-stream upstream-propagating GJW. Since the latter GJW are responsible for most resonances in jets, particularly in screeching and impinging jets, an acoustic source positioned outside the jet is capable of sustaining such resonances. Furthermore, these results suggest that, for control applications, a sound source could be employed in the jet near field to generate free-stream GJW and thereby affect the development of the shear layer near the nozzle lip.

Acknowledgments

This work was granted access to the HPC resources of PMCS2I (Pôle de Modélisation et de Calcul en Sciences de l'Ingénieur et de l'Information) of Ecole Centrale de Lyon and to the resources of CINES (Centre Informatique National de l'Enseignement Supérieur) and IDRIS (Institut du Développement et des Ressources en Informatique Scientifique) under the allocation 2025-2a0204 made by GENCI (Grand Equipement National de Calcul Intensif). It was performed within the framework of the LABEX CeLyA (ANR-10-LABX-0060) within the program *Investissements d'Avenir* (ANR-16-IDEX-0005).

References

[1] Tam, C. K. W., and Hu, F. Q., "On the three families of instability waves of high-speed jets," *J. Fluid Mech.*, Vol. 201, 1989, pp. 447–483. https://doi.org/10.1017/S002211208900100X.

[2] Towne, A., Cavalieri, A. V. G., Jordan, P., Colonius, T., Schmidt, O., Jaunet, V., and Brès, G. A., "Acoustic resonance in the potential core of subsonic jets," *J. Fluid Mech.*, Vol. 825, 2017, pp. 1113–1152. https://doi.org/10.1017/jfm.2017.346.

[3] Tam, C. K. W., and Ahuja, K. K., "Theoretical model of discrete tone generation by impinging jets," *J. Fluid Mech.*, Vol. 214, 1990, pp. 67–87. https://doi.org/10.1017/S0022112090000052.

[4] Edgington-Mitchell, D., and Nogueira, P. A. S., "The guided-jet mode in compressible jets," Tech. Rep. 2023-3647, AIAA Paper, 2023. https://doi.org/10.2514/6.2023-3647.

[5] Maia, I. A., Fiore, M., and Gojon, R., "Tones and upstream-traveling waves in ideally expanded round impinging jets," *Phys. Rev. Fluids*, Vol. 9, No. 8, 2024, p. 083904. https://doi.org/10.1103/PhysRevFluids.9.083904.

[6] Edgington-Mitchell, D., "Aeroacoustic resonance and self-excitation in screeching and impinging supersonic jets - A review," *Int. J. Aeroacoust.*, Vol. 18, No. 2-3, 2019, pp. 118–188. https://doi.org/10.1177/1475472X19834521.

[7] Bogey, C., and Gojon, R., "Feedback loop and upwind-propagating waves in ideally-expanded supersonic impinging round jets," *J. Fluid Mech.*, Vol. 823, 2017, pp. 562–591. https://doi.org/10.1017/jfm.2017.334.

[8] Jaunet, V., Mancinelli, M., Jordan, P., Towne, A., Edgington-Mitchell, D. M., Lehnasch, G., and Girard, S., "Dynamics of round jet impingement," Tech. Rep. 2019-2769, AIAA Paper, 2019. https://doi.org/10.2514/6.2019-2769.

[9] Varé, M., and Bogey, C., "Generation of acoustic tones in round jets at a Mach number of 0.9 impinging on a plate with and without a hole," *J. Fluid Mech.*, Vol. 936, 2022, p. A16. https://doi.org/10.1017/jfm.2022.47.

[10] Jordan, P., Jaunet, V., Towne, A., Cavalieri, A. V. G., Colonius, T., Schmidt, O., and Agarwal, A., "Jet–flap interaction tones," *J. Fluid Mech.*, Vol. 853, 2018, pp. 333–358. https://doi.org/10.1017/jfm.2018.566.

[11] Tam, C. K. W., and Chandramouli, S., "Jet-plate interaction tones relevant to over-the-wing engine mount concept," *J. Sound Vib.*, Vol. 486, 2020, p. 115378. https://doi.org/10.1016/j.jsv.2020.115378.

[12] Gojon, R., Bogey, C., and Mihaescu, M., "Oscillation modes in screeching jets," *AIAA J.*, Vol. 56, No. 7, 2018, pp. 2918–2924. https://doi.org/10.2514/1.J056936.

[13] Edgington-Mitchell, D., Jaunet, V., Jordan, P., Towne, A., Soria, J., and Honnery, D., "Upstream-travelling acoustic jet modes as a closure mechanism for screech," *J. Fluid Mech.*, Vol. 855, 2018, p. R1. https://doi.org/10.1017/jfm.2018.642.

[14] Brès, G. A., Jordan, P., Jaunet, V., Le Rallic, M., Cavalieri, A. V. G., Towne, A., Lele, S. K., Colonius, T., and Schmidt, O. T., "Importance of the nozzle-exit boundary-layer state in subsonic turbulent jets," *J. Fluid Mech.*, Vol. 851, 2018, pp. 83–124. https://doi.org/10.1017/jfm.2018.476.

[15] Bogey, C., "Acoustic tones in the near-nozzle region of jets: characteristics and variations between Mach numbers 0.5 and 2," *J. Fluid Mech.*, Vol. 921, 2021, p. A3. https://doi.org/10.1017/jfm.2021.426.

[16] Zaman, K. B. M. Q., Fagan, A. F., and Upadhyay, P., "Pressure fluctuations due to 'trapped waves' in the initial region of compressible jets," *J. Fluid Mech.*, Vol. 931, 2022, p. A30. https://doi.org/10.1017/jfm.2021.954.

[17] Bogey, C., "Tones in the acoustic far field of jets in the upstream direction," *AIAA J.*, Vol. 60, No. 4, 2022, pp. 2397–2406. https://doi.org/10.2514/1.J061013.

[18] Zaman, K., Bridges, J., Upadhyay, P., and C., B., "Tones due to 'guided jet waves' in the forward arc of high-speed jets," *J. Fluid Mech.*, Vol. 1033, 2026, p. A1. https://doi.org/10.1017/jfm.2026.11315.

[19] Schmidt, O. T., Towne, A., Rigas, G., Colonius, T., and Brès, G. A., "Spectral analysis of jet turbulence," *J. Fluid Mech.*, Vol. 855, 2018, pp. 953–982. https://doi.org/10.1017/jfm.2018.675.

[20] Bogey, C., "Interactions between upstream-propagating guided jet waves and shear-layer instability waves near the nozzle of subsonic and nearly ideally expanded supersonic free jets with laminar boundary layers," *J. Fluid Mech.*, Vol. 949, 2022, p. A41. https://doi.org/10.1017/jfm.2022.776.

[21] Edgington-Mitchell, D. M., Weightman, J. L., Mazharmanesh, S., and Nogueira, P., "Vortices, shocks and non-linear acoustic waves: the ingredients for resonance in impinging compressible jets," *J. Fluid Mech.*, Vol. 1015, 2025, p. A56. https://doi.org/10.1017/jfm.2025.10383.

[22] Powell, A., "The noise of choked jets," *J. Acoust. Soc. Am.*, Vol. 25, No. 3, 1953, pp. 385–389. https://doi.org/10.1121/1.1907052.

[23] Suzuki, T., and Lele, S. K., "Shock leakage through an unsteady vortex-laden mixing layer: application to jet screech," *J. Fluid Mech.*, Vol. 490, 2003, pp. 139–167. https://doi.org/10.1017/S0022112003005214.

[24] Martini, E., Cavalieri, A. V. G., and Jordan, P., "Acoustic modes in jet and wake stability," *J. Fluid Mech.*, Vol. 867, 2019, pp. 804–834. https://doi.org/10.1017/jfm.2019.148.

[25] Nogueira, P. A. S., Cavalieri, A. V. G., Martini, E., Towne, A., Jordan, P., and Edgington-Mitchell, D., "Guided-jet waves," *J. Fluid Mech.*, Vol. 999, 2024, p. A47. https://doi.org/10.1017/jfm.2024.797.

[26] Bogey, C., "Gain in efficiency of jet receptivity to acoustic disturbances with increasing nozzle-lip thickness," *J. Fluid Mech.*, Vol. 997, 2024, p. A71. https://doi.org/10.1017/jfm.2024.849.

[27] Bogey, C., "Numerical simulations of guided jet waves," Tech. Rep. 2025-3078, AIAA Paper, 2025. https://doi.org/10.2514/6.2025-3078.

[28] Bogey, C., "Guided-jet waves generated by an acoustic source in a jet at a Mach number of 0.95," *J. Fluid Mech.*, Vol. 1024, 2025, p. R1. https://doi.org/10.1017/jfm.2025.10910.

[29] Michalke, A., "Survey on jet instability theory," *Prog. Aerosp. Sci.*, Vol. 21, 1984, pp. 159–199. https://doi.org/10.1016/0376-0421(84)90005-8.

[30] Bogey, C., "On noise generation in low Reynolds number temporal round jets at a Mach number of 0.9," *J. Fluid Mech.*, Vol. 859, 2019, pp. 1022–1056. https://doi.org/10.1017/jfm.2018.864.

[31] Bogey, C., and Pineau, P., "Potential-core closing of temporally developing jets at Mach numbers between 0.3 and 2: Scaling and conditional averaging of flow and sound fields," *Phys. Rev. Fluids*, Vol. 4, No. 12, 2019, p. 124601. https://doi.org/10.1103/PhysRevFluids.4.124601.

[32] Mohseni, K., and Colonius, T., "Numerical treatment of polar coordinate singularities," *J. Comput. Phys.*, Vol. 157, No. 2, 2000, pp. 787–795. https://doi.org/10.1006/jcph.1999.6382.

[33] Bogey, C., and Bailly, C., "A family of low dispersive and low dissipative explicit schemes for flow and noise computations," *J. Comput. Phys.*, Vol. 194, No. 1, 2004, pp. 194–214. https://doi.org/10.1016/j.jcp.2003.09.003.

[34] Berland, J., Bogey, C., Marsden, O., and Bailly, C., "High-order, low dispersive and low dissipative explicit schemes for multiple-scale and boundary problems," *J. Comput. Phys.*, Vol. 224, No. 2, 2007, pp. 637–662. https://doi.org/10.1016/j.jcp.2006.10.017.

[35] Tam, C. K. W., and Dong, Z., "Radiation and outflow boundary conditions for direct computation of acoustic and flow disturbances in a nonuniform mean flow," *J. Comput. Acous.*, Vol. 4, No. 2, 1996, pp. 175–201. https://doi.org/10.1142/S0218396X96000040.